Journal of Molecular Graphics and Modelling 121 (2023) 108452

Contents lists available at ScienceDirect

Journal of Molecular Graphics and Modelling

journal homepage: www.elsevier.com/locate/jmgm

Controlled supramolecular interactions for targeted release of Amiodarone drug through Graphyne to treat cardiovascular diseases: An in silico study

Mehvish Perveen [a], N.M.A. Hadia [b,**], Asima Noreen [a], Rana Farhat Mehmood [c], Samia nasr [d,e], I.S. Yahia [d,f,g], Rasheed Ahmad Khera [a,*], Javed Iqbal [a,***]

[a] Department of Chemistry, University of Agriculture, 38000, Faisalabad, Pakistan
[b] Physics Department, College of Science, Jouf University, P.O. Box 2014, Sakaka, Al-Jouf, Saudi Arabia
[c] Department of Chemistry, University of Education, Township, Lahore, 54770, Pakistan
[d] Research Center for Advanced Materials Science (RCAMS), King Khalid University, Abha, 61413, P.O. Box 9004, Saudi Arabia
[e] Chemistry Department, Faculty of Science, King Khalid University, Abha, 61413, P.O. Box 9004, Saudi Arabia
[f] Laboratory of Nano-Smart Materials for Science and Technology (LNSMST), Department of Physics, Faculty of Science, King Khalid University, P.O. Box 9004, Abha, Saudi Arabia
[g] Center of Medical and Bio-Allied Health Sciences Research (CMBHSR), Ajman University, Ajman, P.O. Box 346, United Arab Emirates

ARTICLE INFO

Keywords:
Graphyne
Amiodarone
Drug delivery
DFT
ELF
Cardiovascular drug

ABSTRACT

In the current study, the drug loading ability of graphyne (GY) for the amiodarone (AMD) drug is investigated for the first time. The efficacy of GY as a carrier for amiodarone (a cardiovascular drug) is evaluated by calculating its electronic, energetic, optimized, and excited state properties with help of the density functional theory (DFT). The AMD drug interacted with the GY molecule with an adsorption energy of about −0.19 eV (gas-phase) and −1.92 eV (aqueous phase), suggesting that the AMD@GY complex is stable in water-phase. The HOMO (highest-occupied molecular-orbital) of the AMD@GY complex is concentrated on the AMD drug while the LUMO (lowest-unoccupied molecular-orbital) is centralized on GY with absolute charge separation, indicating charge transfer will occur between AMD and GY. The charge-transfer process is further studied with the aid of charge-decomposition analysis (CDA). The non-covalent interaction analysis (NCI) exposed that non-covalent forces exist between the GY carrier and AMD drug. These non-covalent forces between AMD drug and GY carrier play a significant role in drug unloading at the targeted or diseased site. Likewise, the calculations at excited-state, charge-state (+1 and −1) influence on GY and AMD@GY complex structures, and photo-induced electron transfer analysis (PET) are also studied for the graphyne-based drug-delivery system. According to PET and electron-hole analysis, fluorescence-quenching will occur upon interaction. Overall, it is concluded that graphyne can be exploited as a drug carrier for amiodarone drug delivery. Researchers will be fascinated to look at alternative 2D nanomaterials for drug delivery applications as a result of this theoretical work.

1. Introduction

Cardiovascular diseases (CVDs) are a common cause of mortality worldwide. Every year, almost 17.90 million people are predicted to expire as a result of CVDs, accounting for 31% of all deaths worldwide [1]. Hypertension, a restriction or blockage of blood flow in a specific area, and stroke are all frequent cardiovascular diseases that affect a large number of people. Long-term impairment and death are the most common outcomes of these disorders [2]. There are a variety of drug treatments for these diseases, with the majority of them depending on synthetic active therapeutic agents. Unfortunately, when these drugs are taken, they commonly have significant side effects. As a consequence of this, researchers have done several investigations to find better therapeutics with lowered side effects. In light of this serious scenario, the development of CVDs therapeutics has now become a top priority [3]. In this case, it makes sense to use nanotechnology as a novel and innovative

* Corresponding author.
** Corresponding author.
*** Corresponding author.
E-mail addresses: rasheedahmadkhera@yahoo.com, rasheed.ahmad.khera@uaf.edu.pk (R.A. Khera), javedkhattak79@gmail.com, Javed.iqbal@uaf.edu.pk (J. Iqbal).

https://doi.org/10.1016/j.jmgm.2023.108452
Received 30 December 2022; Received in revised form 2 March 2023; Accepted 8 March 2023
Available online 15 March 2023

approach to preventing cardiovascular disorders [4]. Nanomaterials have been employed as drug carriers, diagnostic, and there-gnostic-agent, in a range of medicinal uses due to their unique properties. For example, therapeutic-agent can be adsorbed, or encapsulated for transport to the target area using nanomaterials [5]. Drug-delivery systems are useful because they can deliver drugs that are either poorly soluble or highly toxic to a target area. Nano-carriers made of nanostructured materials for drug molecules have a preferential effect on cardiac therapies due to their remarkable associations with biological systems, such as their similarity in size to biological systems, rapid penetration, improved water-solubility, which helps in the reduction of cytotoxicity, and long circulation times [6–8]. Researchers are fascinated by the drug loading and distribution property of nanomaterial at specified locations [9,10]. In this line, 2D (two-dimensional nanostructures with a variety of physical, chemical, and mechanical characteristics are promising for cardiovascular diagnostics and treatment. Two-dimensional nanomaterials having a planer form include MoS_2, Bi_2Se_3, MXenes, phosphorene, h-BN as well as graphene and graphene-oxide. These are effective nano-carriers with excellent potential for efficient delivery [11]. The latest member of the carbon-allotropic nanomaterials family, graphyne (GY), offers a variety of unique features such as great thermal stability, low cytotoxicity, a high-surface-area, changeable electric-properties, and improved electric conductivity. GY exhibits sp^2 and sp hybridization [12,13]. A network of nearby benzene rings with an acetylenic-group make up graphyne. Since graphene has a zero energy gap and graphyne has a direct bandgap, it can only be used in electrical circuits to a small extent. To take benefit of its promise of electronic, optical, and mechanical features, scientists have been driven to GY planner carbon structure with regularly organized cavities, changeable electrical-characteristics, and a higher degree of conjunction [14]. GY is also offering a platform for its usage in drug administration due to its unique features including adjustable energy-gap, thermal stability, and high surface-area [15]. For its use in biomedicine, GY interaction with biomolecules, tissues, and various types of cells is crucial. GY, a nanocarrier, can successfully release the drug into the cytosol in response to the stimuli and enter the cell rapidly through endocytosis. The weight ratio of loaded medicine to the carrier is 200% [16] in the case of GY, which makes GY a more efficient nanocarrier than others. Cardiovascular disorders include heart and blood vessel diseases. Angina pectoris, myocardial infarction (MI), atherosclerosis, stroke, and cardiac arrhythmias are some examples of cardiovascular diseases [17]. Cardiac arrhythmias are an illness of cardiac rhythm counting in sudden cessation of the heart's functioning and are correlated to the limited quality of life and exalted death rate. Among many cardiovascular drugs, AMD is the most frequently used antiarrhythmic drug. It is not only permitted to cure potentially fatal ventricular arrhythmias but is also mainly used for the medication of atrial fibrillation [18]. AMD is a class III antiarrhythmic drug. The half-life time of AMD is very long about several weeks. With oral therapy to have full clinical results, it may take 6 weeks. After discontinuation of AMD therapy, pharmacological effects may also persist for 1–3 months [19]. There are several non-cardiac side effects of AMD on different organs including the skin, peripheral nervous system, eye, liver, and lungs [20]. To reduce toxicity by targeted transferring of the drug, the design of nanostructures for drug-loading is extremely important [21].

Dongwie et al. [22], investigated the catalytic-activity and stability of transition metal atoms supported on graphdiyne monolayers. First-principles calculations revealed that most of these transition-metal atom-based graphdiyne monolayers showed the best catalytic-activity for the nitrogen reduction reaction. Furthermore, the potential of alkaline-earth metal-based graphene and graphitic carbon-nitride is also explored in the field of heterogeneous-catalysis. First-principles calculations were performed to evaluate the effectiveness of alkaline-earth metal atoms-based active-centers in heterogeneous catalysis [23,24].

Karim et al. [25], investigated the theranostic-potential of alkaline-earth metal-based phosphorene. The electronic properties of ifosfamide (an anticancer drug) loaded phosphorene molecules were calculated using Density functional theory calculations. The results suggested that alkaline earth metal doped phosphorene complex with ifosfamide drug is a potential candidate for drug delivery and photothermal therapy. Furthermore, Allangawi et al. [26] accomplished first principles calculations and DFT simulations to investigate the electronic-properties of the boron-doped covalent organic framework (COF) for an anticancer drug; tegafur. Overall, the results showed that triazine-based COF can be used as a carrier for delivery of tegafur drug to treat cancer.

Herein, for the first time, the effectiveness of graphyne (GY) for the targeted transport of therapeutic-agent amiodarone (AMD) is examined utilizing the Density Functional Theory (DFT) and TD-DFT approach. The AMD drug is loaded onto nanostructure-cavities of the GY carrier molecule.

2. Computational details

By using the DFT approach [27] with Gaussian 09 software all theoretical calculations were accomplished [28]. Molecular structures were optimized using the CAM-B3LYP method [29,30] with the basis set of Lanl2DZ [31]. The CAM-B3LYP functional hybrid is more useful and accurate for DFT calculations. B3LYP, which is good at describing electron properties with a 20% HF factor, still underestimates long-range dispersion-corrections [32]. While CAM-B3LYP can estimate long range-corrections [33]. Furthermore, CAM-B3LYP, a modified version of B3LYP, is preferable to B3LYP because it shows a greater degree of precision [34] in charge transfer and produces reliable results in amiodarone drug delivery.

The computation of excited state properties was made at TD-B3LYP/Lanl2DZ by using TD-DFT (Time dependent-DFT) [35]. The AMD@GY complex's most stable configuration was chosen after considering various possible structures. Frequency calculations were performed to confirm the true minima of complex structures with no imaginary-frequency. Another valuable factor for understanding the interaction between different species that leads to complex formation is adsorption energy [36]. Optimized complex absorption energy was calculated using the following equation;

$$Ead = E_{AMD@GY} - (E_{GY} + E_{AMD}) \quad (1)$$

Where $E_{AMD@GY}$ is the energy of complex AMD@GY, E_{GY} represents the energy of GY, and E_{AMD} shows the energy of amiodarone. The E_{ad} represents the adsorption energy.

The solvent effect was analyzed by IEF-PCM (integral-equation formalism with polarizable-continuum model) for the study of the nature of the interaction of AMD drug with GY [37]. As water performs a central role in the living system it is selected as a solvent. By taking water as a solvent, it is mandatory to understand its influence on the stability of the AMD@GY [38,39]. Stability is explained in terms of the solvation energy of complex AMD@GY calculated by using equation (4);

$$\Delta E_{Solvation} = E_{SOl} - E_{gas} \quad (4)$$

The solvation-energy of the AMD@GY complex is represented by $\Delta E_{Solvation}$. Where E_{sol} and E_{gas} are energies in the water and gas phase, respectively. Some necessary calculations such as chemical-reactivity descriptors and energies of HOMO-LUMO orbitals were calculated for AMD, GY, and AMD@GY complex. After complex molecule formulation variations among the electron density of GY were calculated through the Electron localization function (ELF). Charge-transfer between AMD and GY was analyzed using charge-decomposition analysis (CDA). Intermolecular orbital-interaction like charge mobility from one part of the complex to other was computed using NBO analysis [40]. The electronic excitations from AMD to graphyne and graphyne to AMD were also considered. Furthermore, based on TD-DFT calculations, gas and aqueous phase UV–Vis absorption-spectra of AMD, GY, and AMD@GY

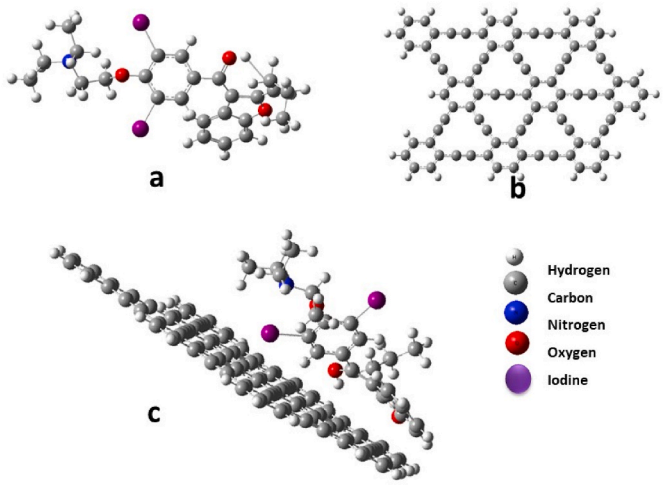

Fig. 1. Optimized geometries of (a) AMD, (b) GY, and (c) complex AMD@GY complex.

complex were calculated [41,42]. The NCI, PET and charge-transfer analysis were also considered. In this study, the effect of surface-charges on analyzed drug-delivery system was also checked.

Processes of charge-transfer and photoinduced electron-transfer in living systems are of significant consequence because dimensions of some processes such as phosphorescence and fluorescence are influenced by these phenomena e.g., charge or electron shifting to fluorophore from chelator causes the fluorescence quenching [43,44]. Fluorescence and optical recognition of nanoparticles and therapeutic agents have an important role in efficient drug delivery [45].

3. Results and discussion

3.1. Optimized structure and adsorption energy

The optimized structures of GY, AMD, and AMD@GY are presented in Fig. 1. The optimized-molecular structures of the AMD@GY indicate that the AMD drug prefers to interact via Hydrogen atoms to the Carbon atoms of the GY molecule [37]. Three aliphatic protons of AMD interacted via the distance of 4.03 Å, 3.47 Å, and 3.50 Å with the GY carrier. The AMD@GY complex shows an adsorption-energy [46] value of −0.19 eV (gas-phase) and −1.92 eV (aqueous-phase) suggesting that the AMD@GY is stable in the water-phase. The negative value of Ead of AMD@GY (−1.92 eV) signifies that the amiodarone molecule is effectively adsorbed on the GY and the AMD@GY formation is thermodynamically-favorable process. However, the adsorption of AMD on the GY surface is not so strong that it would cause problems in drug-desorption, as the AMD molecule interacted non-covalently with the GY molecule. So with this Ead value amiodarone drug will easily off-load from the GY. However, some approaches for the release of therapeutic agent from carrier-surface can also be used. The light-triggered method will be useful for controlled drug-release due to

Table 1
The $E_{(HOMO)}$, $E_{(LUMO)}$, band-gap, λ_{max}, dipole-moment, μ (chemical-potential), η (hardness), S (softness), and ω (global-electrophilicity) of GY, AMD and AMD@GY complex in gas-phase.

	E_{HOMO}	E_{LUMO}	E_g (eV)	λ_{max} (nm)	Dipole moment (D)	μ (eV)	η (eV)	S (eV^{-1})	ω (eV)
GY	−5.50	−2.88	2.62	511	0.21	−4.19	1.31	0.38	6.69
AMD	−5.22	−2.14	3.08	416	1.23	−3.68	1.54	0.32	4.39
AMD@GY complex	−5.23	−2.90	2.33	503	0.38	−4.06	1.17	0.43	7.04

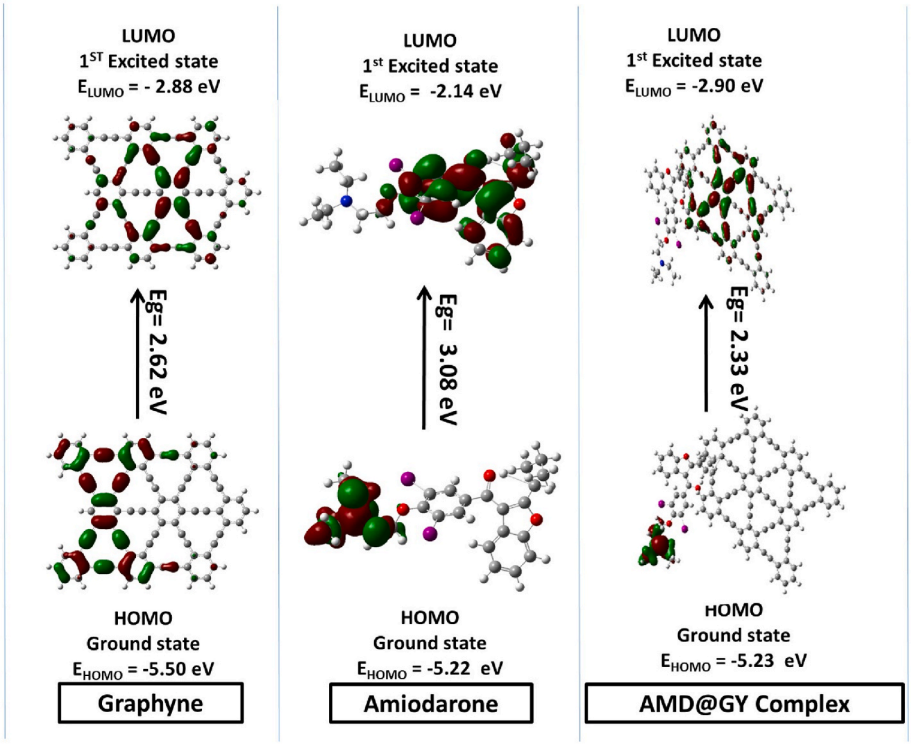

Fig. 2. Visual illustration of HOMO-LUMO of GY, AMD drug, and AMD@GY.

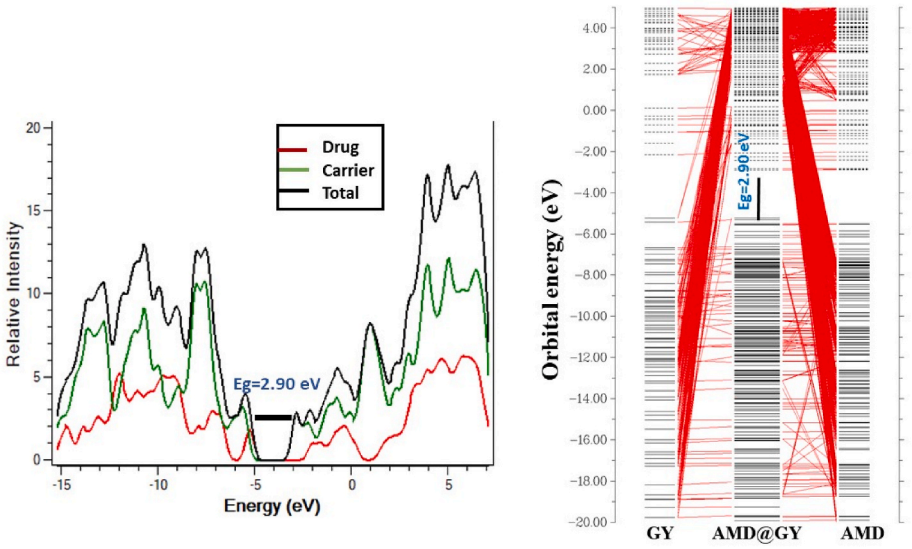

Fig. 3. **(a)** Density of states and **(b)** CDA of AMD@GY complex.

its harmless nature [47]. The irradiation of visible-light will be helpful as it will cause a photothermal-effect that will contribute in controlled drug-release at its targeted-area [45]. Table 1 shows that the dipole moments of AMD, GY, and AMD@GY are 1.237, 0.218, and 0.383 D, correspondingly. The dipole-moment is increased to 0.383 D after complex-AMD@GY formation. The solubility of the AMD@GY complex towards water improves with the rise in the dipole moment.

3.2. HOMO-LUMO analysis

HOMO-LUMO investigations help us to understand the system's stability and reactivity. The HOMO-LOMO gap denotes the amount of energy necessary for a successful drug-carrier interaction. The energies related to the HOMO and the LUMO of the GY, AMD, and AMD@GY complex are the most important factors in evaluating the drug-carrier interaction. The HOMO of AMD@GY complex is concentrated only on AMD while LUMO is only centralized on GY with absolute charge separation, indicating charge transfer will occur between AMD drugs and GY (see Fig. 2). The lowest unoccupied MOs and highest occupied MOs energies $E_{(LUMO)}$, $E_{(HOMO)}$, band gap, and their λ_{max} are illustrated in Table 1. The $E_{(HOMO)}$ and $E_{(LUMO)}$ of GY is −5.50 eV and −2.88 eV respectively, and its energy gap is 2.62 eV. The $E_{(HOMO)}$ and $E_{(LUMO)}$ of AMD are −5.52 and −2.14 eV correspondingly, with the Eg value of 3.08 eV. The HOMO-LUMO energies of AMD@GY-complex are −5.23 eV and −2.90 eV respectively, with Eg (band-gap) of 2.33 eV which is smaller than the GY (2.62 eV) and AMD (3.08 eV). Lesser-amount of energy is needed for the transition from the low-energy level to the higher level (excited state) as the energy band gap of the complex (AMD@GY) is smaller than the carrier (graphyne). The E_{HOMO} of the AMD@GY complex is analogous to the AMD energy, while the E_{LUMO} is similar to the GY energy. This association is almost exclusively reliable with the point that HOMO is limited on AMD while the LUMO of complex-system is restricted on graphyne, demonstrating that AMD is an electron-donor and GY is an electron-acceptor in the AMD@GY complex. The GY showed λ_{max} at 511 nm whereas the AMD@GY complex showed λ_{max} at 503 nm.

3.3. CDA and DOS analysis

The most important analysis for studying donor-acceptor interactions and their molecular-orbitals interaction in the system is charge-decomposition analysis (CDA) [48]. As illustrated in Fig. 3b, new MOs are added during the formation of AMD@GY complex (by fusion of energy levels of fragments) that minimize bandgap (Eg), increased E_{HOMO} (−5.23 eV), and lowered the E_{LUMO} (−2.90 eV) as shown from the diagram of CDA. This diagram featured that energy-levels are added in the complex and reduced Eg between the energy-levels which further promotes the charge-transfer. These findings represent the effective attachment of AMD on the graphyne nanocarrier. And CDA results are further strengthened by the DOS (density of states) spectrum (Fig. 3a). Both the DOS spectrum and CDA results showed how the formation of new MOs in the AMD@GY helped in the decrease of the energy-gap (2.33 eV) and resulted in charge-transferal among the two components.

3.4. Reactivity-descriptors (μ, η, s, ω) and dipole-moment

In terms of reactivity descriptors, the stability and electronic characteristics of the complex, e.g., electron transfer are also well explained. A hard molecule has a large H-L gap (HOMO-LUMO gap), while a soft compound has a smaller H-L gap. Molecular stability and hardness are also related to the fact that the system with the small H-L gap is more reactive. The AMD@GY (0.43 eV^{-1}) is found softer than GY (0.38 eV^{-1}) and AMD (0.32 eV^{-1}), as shown in Table 1. The hardness (η) of the AMD@GY (1.17 eV) was lesser than that of GY (1.31 eV) and AMD (1.54 eV). The chemical potential of the AMD@GY (−4.06 eV) was lower than that of the GY (−4.19 eV) but higher than that of the AMD (−3.68 eV). The negative chemical potential value signifies that the AMD@GY complex is stable. The electrophilicity-index quantifies that complex-system gaining extra charges from its surroundings to maintain system stability. The high potential of the AMD@GY complex, lower hardness, and higher magnitude of electrophilicity-index specifically indicate that this complex can be used for antiarrhythmic drug delivery at the targeted site [49].

3.5. Non-covalent interaction analysis

The NCI analysis is a successful method for visualizing non-covalent interactions (e.g., van-der Waals-interactions (vdWs), steric repulsions, and H-bonding) in non-covalently interacting molecules [50]. Weak interactions between the AMD and the GY are essential for targeted delivery. The NCI graph is designed between reduced-density gradient (RDG) and sin λ_2 (ρ). The sin λ_2 (ρ) is the critical point of the NCI scatter plot and is used to detect the chemical bonding of the AMD@GY-complex. The vdWs interactions are depicted by spikes close to the zero-area of sin λ2(ρ). The non-covalent interactions between graphyne and the AMD drug are also illustrated by the 3D color-filled

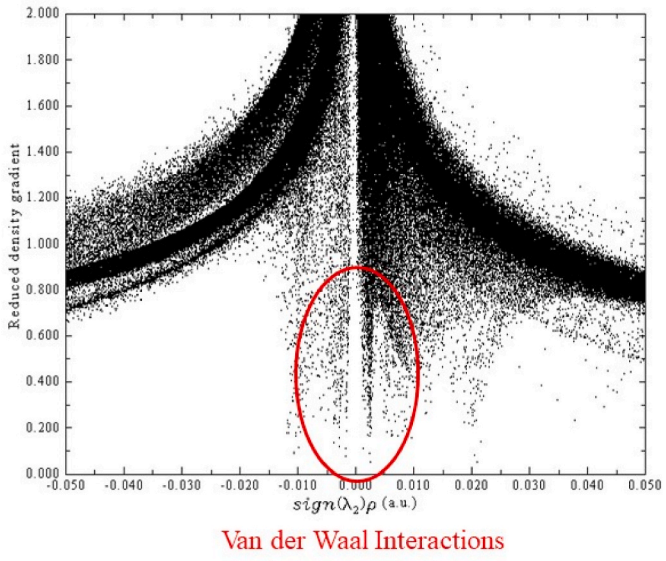

Fig. 4. The NCI analysis of AMD@GY complex.

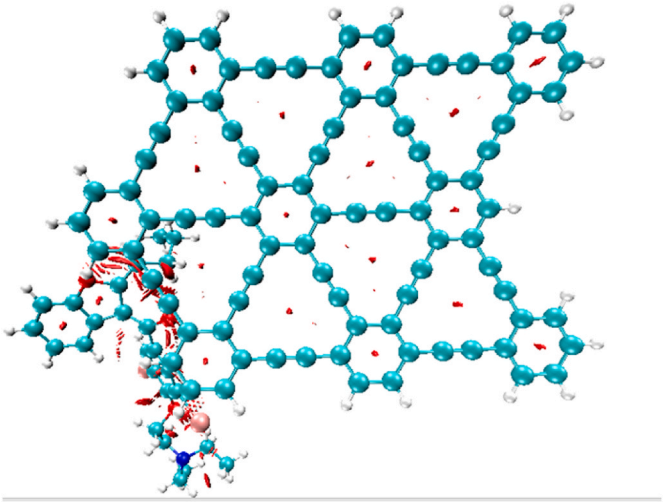

Fig. 5. 3D iso-surface image of AMD@GY complex.

isosurface given in Fig. 4. The weak-forces (C···H) observed in the geometrical study of AMD@GY are in agreement with NCI results. The Carbon and Hydrogen atoms in the AMD@GY complex come from GY and AMD, respectively [51] (see Fig. 5).

3.6. ELF and NBO analysis

Electron localization function (ELF) images for GY and AMD@GY are illustrated in Fig. 6a and b. ELF electron-density plots are used to monitor the variations in the electron-density of graphyne after the AMD@GY complex-formulation. During the formation of the AMD@GY, the electron-density of the GY was appreciably altered, as seen from these plots.

The NBO (natural-bond orbital analysis) [52] is an excellent parameter for examining intra-molecular and inter-molecular interactive forces, as well as charge transfer in molecular-systems [53]. Electronic transitions or charge transfers from graphyne to drug and drug molecules to graphyne, including inside the graphyne carrier, are also put into consideration for NBO analysis and are easily interpreted using ELF electron-density plots. Table 2 illustrates the energy-changes for internal-transitions in the graphyne during the formation of the complex (AMD@GY).

3.7. Effect of solvent

This study looked at the influence of water on the interactions between AMD and GY, along with their impact on the stability and aqueous solubility of the AMD@GY. Because water is the most important component in the biological-system, it is selected as the solvent for a method to mimic the body's situation. In the water, the predicted adsorption energy for AMD@GY is −1.92 eV. This negative Ead value

Table 2
NBO-analysis of GY and AMD@GY complex (energy unit; Kcal mole^{-1}).

AMD→ GY	Energy	GY → GY	Before	After
$\sigma_{C6\text{-}C14} \rightarrow LP^*_{H\text{-}50}$	0.81	$\sigma_{C1\text{-}C2} \rightarrow \sigma^*_{C1\text{-}C6}$	1.59	2.27
$\sigma_{O11\text{-}C14} \rightarrow LP^*_{H\text{-}50}$	3.65	$\sigma_{C1\text{-}C2} \rightarrow \sigma^*_{C2\text{-}C3}$	2.59	2.46
$\sigma_{C14\text{-}C30} \rightarrow LP^*_{H\text{-}50}$	0.08	$\sigma_{C1\text{-}C6} \rightarrow \sigma^*_{C1\text{-}C2}$	1.72	2.81
$\sigma_{C41\text{-}C42} \rightarrow LP^*_{H\text{-}50}$	0.11	$\sigma_{C1\text{-}C6} \rightarrow \sigma^*_{C5\text{-}C6}$	1.54	2.64
$\sigma_{C41\text{-}C60} \rightarrow LP^*_{H\text{-}50}$	0.43	$\sigma_{C2\text{-}C3} \rightarrow \sigma^*_{C1\text{-}C2}$	2.37	2.32
LP (1) $_{O11} \rightarrow LP^*(1)_{H\text{-}50}$	0.60	$\sigma_{C2\text{-}C3} \rightarrow \sigma^*_{C3\text{-}C4}$	2.36	3.61
GY→ AMD		$\sigma_{C3\text{-}C4} \rightarrow \sigma^*_{C2\text{-}C3}$	2.36	3.64
$LP_{H\text{-}50} \rightarrow \sigma^*_{C1\text{-}C6}$	0.08	$\sigma_{C3\text{-}C4} \rightarrow \sigma^*_{C4\text{-}C5}$	1.59	2.16
$LP_{H\text{-}50} \rightarrow \sigma^*_{C4\text{-}C5}$	0.05	$\sigma_{C4\text{-}C5} \rightarrow \sigma^*_{C5\text{-}C6}$	1.54	2.04
$LP_{H\text{-}50} \rightarrow \sigma^*_{C6\text{-}C14}$	0.26	$\sigma_{C4\text{-}C5} \rightarrow \sigma^*_{C3\text{-}C4}$	1.72s	2.32
$LP_{H\text{-}50} \rightarrow \sigma^*_{O11\text{-}C14}$	14.72	$\sigma_{C5\text{-}C6} \rightarrow \sigma^*_{C1\text{-}C6}$	1.54	2.66
$LP_{H\text{-}50} \rightarrow \sigma^*_{C14\text{-}C30}$	0.95	$\sigma_{C5\text{-}C6} \rightarrow \sigma^*_{C4\text{-}C5}$	1.54	2.48
$LP_{H\text{-}50} \rightarrow \sigma^*_{C29\text{-}C30}$	0.20	$\sigma_{C49\text{-}C54} \rightarrow \sigma^*_{C37\text{-}C53}$	3.87	4.14
$LP_{H\text{-}50} \rightarrow \sigma^*_{C30\text{-}C31}$	0.13	$\sigma_{C50\text{-}C51} \rightarrow \sigma^*_{C51\text{-}C52}$	2.39	2.72
$LP_{H\text{-}50} \rightarrow \sigma^*_{C40\text{-}H49}$	0.14	$\sigma_{C53\text{-}C54} \rightarrow \sigma^*_{C36\text{-}C37}$	4.25	5.37
$LP_{H\text{-}50} \rightarrow \sigma^*_{C41\text{-}C42}$	1.60	$\sigma_{C55\text{-}C56} \rightarrow \sigma^*_{C57\text{-}C58}$	2.67	3.88
$LP_{H\text{-}50} \rightarrow \sigma^*_{C41\text{-}H59}$	0.10	$\sigma_{C57\text{-}C58} \rightarrow \sigma^*_{C58\text{-}C59}$	1.35	2.87
$LP_{H\text{-}50} \rightarrow \sigma^*_{C72\text{-}C60}$	0.11	$\sigma_{C59\text{-}C60} \rightarrow \sigma^*_{C58\text{-}C63}$	2.61	3.73

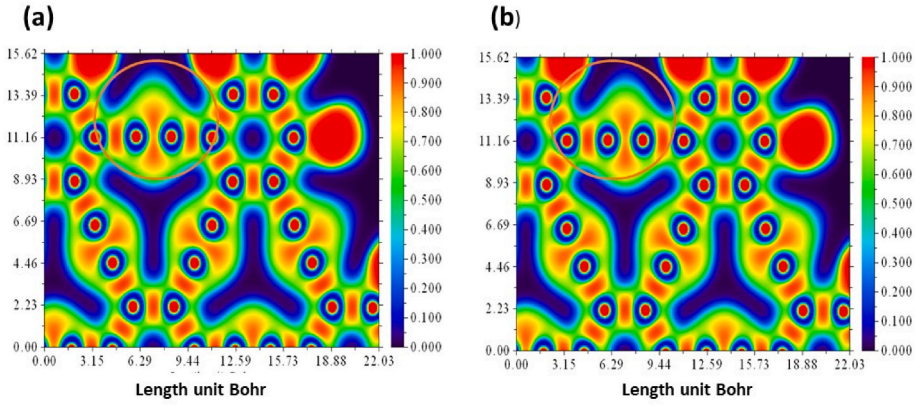

Fig. 6. (a). ELF of Graphyne **6 (b)**. ELF of AMD@GY complex.

Table 3
HOMO-LUMO energies, Eg, λ_{max}, dipole-moment, chemical potential(μ), hardness (η), softness (S), and global-electrophilicity (ω) of GY, AMD, and AMD@GY in the solvent.

	E_{HOMO}	E_{LUMO}	E_g (eV)	λ_{max} (nm)	Dipole moment (Debye)	μ (eV)	η (eV)	S (eV^{-1})	ω (eV)
GY	−5.80	−3.24	2.56	503	0.47	−4.52	1.28	0.39	7.98
AMD	−5.44	−2.17	3.27	410	1.65	−3.80	1.64	0.30	4.40
AMD@GY complex	−5.44	−3.24	2.2	597	1.07	−4.34	1.1	0.45	8.56

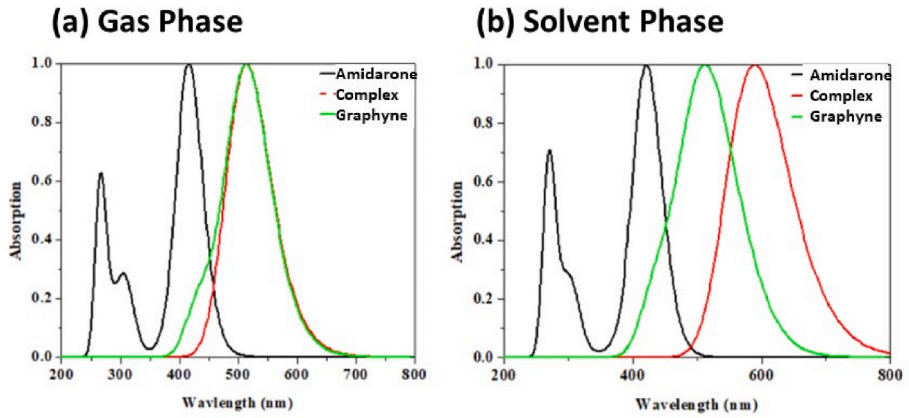

Fig. 7. Absorption-spectra of AMD, GY, and AMD@GY complex, **(a)** gas **(b)** water.

indicates that AMD adsorption on the surface GY is exothermic. The Ead of the AMD@GY in the aqueous-phase (−1.92 eV) is higher than in the gas media (−0.19 eV), suggesting that the stability is somewhat increased in water.

The solvation-energies for AMD, GY, and AMD@GY were also calculated. The solvation-energies of the AMD and the GY were −0.38 eV and −0.6 eV, correspondingly. The AMD@GY-complex has a solvation-energy of −0.98 eV. The computed Esolvtion for drug, carrier, and complex are all negative, indicating that complex-solvation is a spontaneous process referring to the AMD@GY complex's water stability. Table 3 shows the energy of HOMO-LUMO, band gaps, chemical-reactivity descriptors, and dipole-moments of graphyne, AMD, and AMD@GY in the solvent phase. The H-L energies and band-gap of AMD, GY, and AMD@GY show minor variations in the solvent-phase in comparison to gas-media. By converting the gaseous phase to aqueous media, water addition greatly enhanced the polarity or dipole-moment of AMD, GY, and AMD@GY complex. The increased dipole-moments in the solvent-phase show that the AMD@GY complex has improved solubility in the aqueous phase than in gas-media. Molecular stability and hardness are also related to the fact that the system with the small band-gap is more reactive. Chemical-softness (s) values for graphyne, AMD, and AMD@GY complex are increased, while chemical-hardness is decreased somewhat. This indicates that these molecules are more reactive in the aqueous media than in the gas-phase. The fact that the electrophilicity-index (ω) for the AMD@GY complex is 8.56 eV specifies that the complex system is chemically-stable in the solvent phase. Overall outcomes suggested that the AMD@GY can be efficiently employed as a drug-transport vehicle.

3.8. UV–Vis absorption spectra

The theoretically-calculated UV–Vis spectra of AMD, GY, and AMD@GY-complex are shown in Fig. 7. The AMD@GY showed max-absorption at around 503 nm, which is significantly higher than AMD's (λ max) at 416 nm. The λ_{max} at 503 nm for the AMD@GY is parallel to 2.33 eV, which coincides with the energy gap among HOMO-LUMO. This relation shows that absorption at 503 nm is accountable for the transition from HOMO to LUMO. The AMD, GY, and AMD@GY have

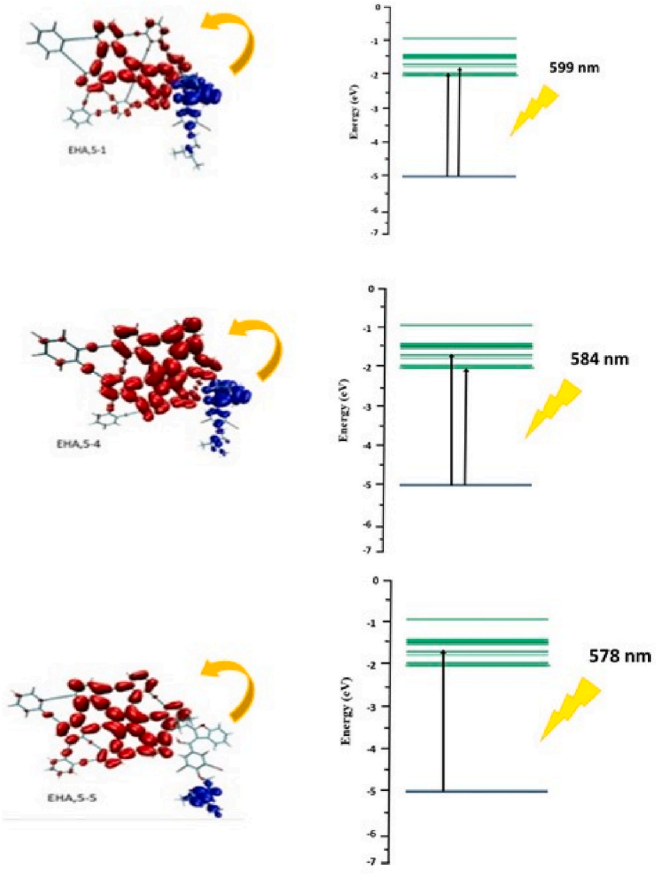

Fig. 8. Electron-hole orbitals and PET process for 1–3 excited states.

absorbance values of 410 nm, 537 nm, and 597 nm, respectively in the water-phase. It was determined that the excitation of electrons occurs at 503 nm in the gas and 597 nm in the water, emphasizing that the charge

Table 4
EH analysis of 1–3 excited-states of complex AMD@GY.

Excited states of AMD@GY	1	2	3
λmax (nm)	599.3	584.4	578.1
ΔE (eV)	2.069	2.122	2.144
F	0.0017	0.0062	0.0004
D $_{Index}$ (Å)	7.972	9.078	15.257
S	0.27414	0.29377	0.07964
Transition mode	CT	CT	CT

is de-localized from AMD to GY. All these were reported in the Visible-region of the light, thus this material can be used for fluorescence and calorimetric-measurement, which helps in finding the exact target location [54].

3.9. Photo-induced electron-transfer analysis

The detailed review of the de-localization of unpaired electrons i.e., the excitation of any molecule from a lower-state to a higher energy-state, revealed useful information about biological processes [55]. The electron-transferring phenomena in excited states of the AMD@GY-complex can be studied using electron-hole theory. The electron-hole for 1–3 excited-states for AMD@GY-complex has presented in Fig. 8. Red-colored orbitals are electrons (AMD) and blue-color orbitals are holes (GY).

Graphyne functions as fluorophore and AMD as chelator and charge-transfer occurs from AMD (chelator) to GY (fluorophore). The distance between fragment molecules determines whether the PET phenomenon takes place or not. The manifestation of PET is certain if electron-hole orbitals are parted by good approximation. Results computed with the aid of electron-hole theory are provided in Table 4. The Charge transfer lengths (CT) can be measured by the distance (D $_{Index}$) between the centroid of the electron or hole. Depending on the distance between

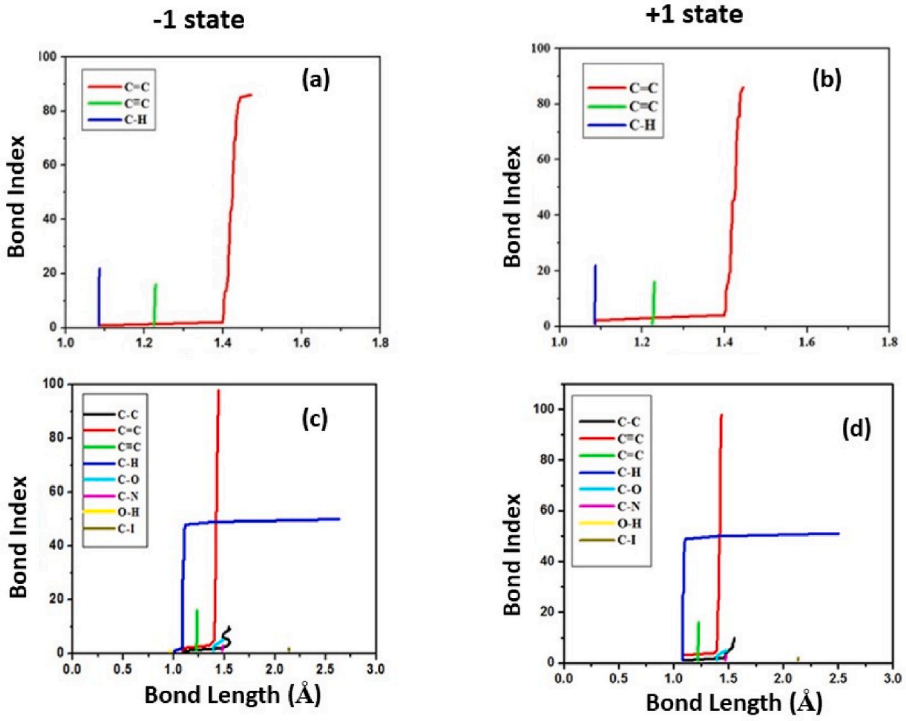

Fig. 9. Bond-lengths of (a) GY^{1-} and (b) GY^{1+} (c) $AMD@GY^{-1}$(d) $AMD@GY^{1+}$ complex.

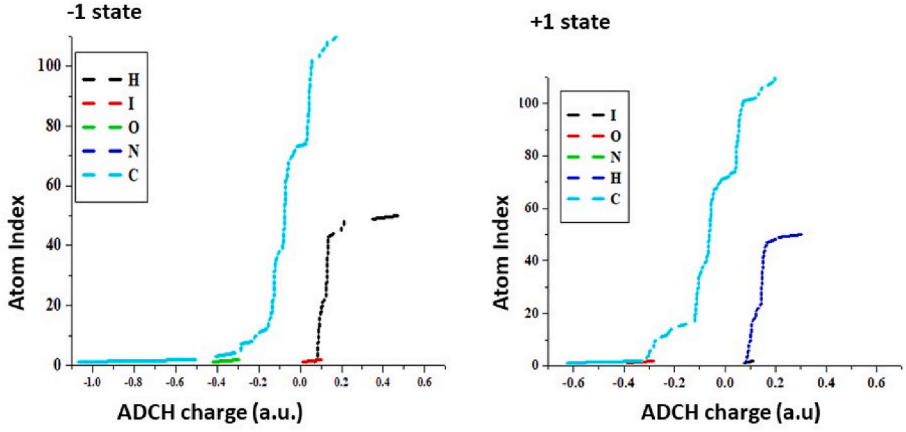

Fig. 10. ADCH charges of (a) $AMD@GY^{1-}$ complex and (b) $AMD@GY^{1+}$ complex.

orbitals, electronic excitations can be de-localized (longer CT) and localized (shorter CT) in nature. Fig. 10 shows electron-hole orbitals for the first three excited-state. The orbitals of excited-states have distances of 7.972 Å, 9.078 Å, and 15.257 Å, correspondingly demonstrating that delocalized excitations will occur. Table 4 shows the values of overlapping electron-hole integral (s). The smaller values S for 1,2, and 3 excited-states (i.e., 0.27414, 0.29377, and 0.07964) represent high charge-transfer length.

3.10. Effect of surface-charge

Positive and negative charges on the surface help in molecules attachment with several components for example cell and plasma-membranes in human-body [56] The effect of +1 charge and −1 charge on the bond lengths of GY and its complex AMD@GY was reflected by using DFT computational approach (see Fig. 9). The carbon double-bond carbon (C=C) bond lengths are 1.09 Å and 1.22 Å correspondingly in the graphyne^{1-} and graphyne^{1+}. The C≡C bond distances in GY^{1-} and GY^{1+} are 1.03 Å and 1.04 Å. When the AMD drug is adsorbed at GY-surface then the bond lengths of -C-C of GY^{1-} and GY^{1+} are 1.44 Å and 1.43 Å. The bond-lengths of –C≡C- in AMD@GY^{1-} complex and AMD@GY^{1+} are 1.224 Å, and 1.225 Å, correspondingly. The bond lengths of C=O are 1.39 Å and 1.38 Å in AMD@GY^{1-} and AMD@GY^{1+}, respectively. The charge on C-atoms of AMD@GY^{1+} and AMD@GY^{1-} are zero a.u. and -0.5 a.u. correspondingly. Atomic-dipole moment corrected-Hirshfeld charge (ADCH) calculations on the surface of AMD@GY$^{1+/1-}$ are useful for the recognition of active-sites which will assist in more surface-attachments. The ADCH charges of AMD@GY^{1+} complex and AMD@GY^{1-} complex are shown in Fig. 10.

4. Conclusion

The therapeutic effectiveness of graphyne (GY) for the effective preferred targeted administration of a cardiovascular drug, amiodarone (AMD) is investigated in this study. The DFT and TD-DFT approach is utilized to determine the quantum-characteristics of the AMD, GY, and AMD@GY-complex at the ground and excited phase since modeling nearly provides the same results as experimental values. The Ead for AMD@GY is about −0.19 eV in the gas phase and −1.92 eV in water-phase. The Ead value represents that the AMD@GY complex is stable in water-phase. The process of charge-transfer is confirmed by the formation of HOMO on AMD and LUMO on GY. The existence of non-covalent inter-molecular interactions such as vdWs forces has been validated by the visual depiction of the NCI-plot. These weak forces aid in the effective un-loading of AMD drug to the targeted-area. The types of transitions that occur from GY to AMD or AMD to GY are explained by natural bond orbital analysis. For various excited states, the PET process is well described using electron-hole theory. The GY, AMD, and AMD@GY complexes have maximum absorption wavelengths that are quite similar to experimental results. Furthermore, the charge-effect studies demonstrated less distortion in geometry and showed the complex molecule's active sites. Simply stated, the carrier GY exhibits good coordination with the cardiovascular-drug; AMD and may be employed to deliver AMD drug to a definite target-region. The exciting horizons of GY (covered in this work) will be useful in the future since it has the efficiency for remarkable medicinal applications and opens a new frontier for investigators to address drug delivery challenges.

Declaration of competing interest

The authors declare that they have no known competing financial interests or personal relationships that could have appeared to influence the work reported in this paper.

Data availability

Data will be made available on request.

Acknowledgement

The authors acknowledge and thank the Research Center for Advanced Materials Science (RCAMS)" at King Khalid University, Saudi Arabia, for funding this work under the grant number RCAMS/KKU/016-22.

References

[1] Y. Cho, et al., Use of statin for the primary prevention of cardiovascular outcomes in elderly patients: a propensity-matched cohort study, Atherosclerosis (2021).
[2] H.C. McGill Jr., C.A. McMahan, S.S. Gidding, Preventing heart disease in the 21st century: implications of the Pathobiological Determinants of Atherosclerosis in Youth (PDAY) study, Circulation 117 (9) (2008) 1216–1227.
[3] H. Rachmawati, et al., In vitro study on antihypertensive and antihypercholesterolemic effects of a curcumin nanoemulsion, Sci. Pharm. 84 (1) (2016) 131–140.
[4] A. Radomska, J. Leszczyszyn, M.W. Radomski, The nanopharmacology and nanotoxicology of nanomaterials: new opportunities and challenges, Adv. Clin. Exp. Med. 25 (1) (2016) 151–162.
[5] M. Mauricio, et al., Nanoparticles in medicine: a focus on vascular oxidative stress, Oxid. Med. Cell. Longev. 2018 (2018).
[6] S. Logothetidis, Nanomedicine: the medicine of tomorrow, in: Nanomedicine and Nanobiotechnology, Springer, 2012, pp. 1–26.
[7] B.E. Rabinow, Nanosuspensions in drug delivery, Nat. Rev. Drug Discov. 3 (9) (2004) 785–796.
[8] D. Horn, J. Rieger, Organic nanoparticles in the aqueous phase—theory, experiment, and use, Angew. Chem. Int. Ed. 40 (23) (2001) 4330–4361.
[9] O.C. Farokhzad, R. Langer, Impact of nanotechnology on drug delivery, ACS Nano 3 (1) (2009) 16–20.
[10] A. Bianco, K. Kostarelos, M. Prato, Applications of carbon nanotubes in drug delivery, Curr. Opin. Chem. Biol. 9 (6) (2005) 674–679.
[11] C. Zhu, D. Du, Y. Lin, Graphene-like 2D nanomaterial-based biointerfaces for biosensing applications, Biosens. Bioelectron. 89 (2017) 43–55.
[12] Y. Du, et al., Fundament and application of graphdiyne in electrochemical energy, Accounts Chem. Res. (2020).
[13] R. Wei, S. Jameh-Bozorghi, γ-graphyne and its boron nitride analogue as nanocarriers for anti-cancer drug delivery, Mol. Phys. (2019) 1–8.
[14] I. Munir, et al., Therapeutic potential of graphyne as A new drug-delivery system for daunorubicin to treat cancer: a DFT study, J. Mol. Liq. (2021), 116327.
[15] J. Jin, et al., Graphdiyne nanosheet-based drug delivery platform for photothermal/chemotherapy combination treatment of cancer, ACS Appl. Mater. Interfaces 10 (10) (2018) 8436–8442.
[16] M.A. Khan, et al., Controlled supramolecular interaction to enhance the bioavailability of hesperetin to targeted cancer cells through graphyne: a comprehensive in silico study, RSC Adv. 12 (10) (2022) 6336–6346.
[17] E.G. Nabel, Cardiovascular disease, N. Engl. J. Med. 349 (1) (2003) 60–72.
[18] K.C. Koskinas, et al., Ranolazine enhances the efficacy of amiodarone for conversion of recent-onset atrial fibrillation, Europace 16 (7) (2014) 973–979.
[19] P.C. Wiener, et al., Unforeseen consequences: class III antiarrhythmic amiodarone stimulated increase in prostate-specific antigen, HeartRhythm Case Rep. 7 (5) (2021) 267.
[20] E.H. Vyskocilova, et al., Therapeutic monitoring of amiodarone: pharmacokinetics and evaluation of the relationship between effect and dose/concentration, Biomedical Papers of the Medical Faculty of Palacky University in Olomouc 161 (2) (2017).
[21] W. Cui, J. Li, G. Decher, Self-assembled smart nanocarriers for targeted drug delivery, Adv. Mater. 28 (6) (2016) 1302–1311.
[22] D. Ma, et al., Computational evaluation of electrocatalytic nitrogen reduction on TM single-, double-, and triple-atom catalysts (TM= Mn, Fe, Co, Ni) based on graphdiyne monolayers, J. Phys. Chem. C 123 (31) (2019) 19066–19076.
[23] D. Wu, et al., Atomically dispersed alkaline-earth metals as active centers for CO2 electroreduction to exclusively produce formate, Small Structures (2022), 2200358.
[24] D. Wu, et al., Catalytic active centers beyond transition metals: atomically dispersed alkaline-earth metals for the electroreduction of nitrate to ammonia, J. Mater. Chem. (2023).
[25] H. Karim, et al., A DFT investigation on theranostic potential of alkaline earth metal doped phosphorenes for ifosfamide anti-cancer drug, Appl. Surf. Sci. 596 (2022), 153618.
[26] A. Allangawi, et al., High drug carrying efficiency of boron-doped Triazine based covalent organic framework toward anti-cancer tegafur; a theoretical perspective, Computat. Theoret. Chem. 1220 (2023), 113990.
[27] R. Parr, W. Yang, Density-Functional Theory of Atoms and Molecules, Oxford University Press, Oxford, 1989.
[28] M. Frisch, et al., Gaussian 09 Revision D. 01, 2014.
[29] A. Becke, Density-functional thermochemistry. III. The role of exact exchange, J. Chem. Phys. 98 (1993) 5648.

[30] C. Lee, W. Yang, R.G. Parr, Development of the Colle-Salvetti correlation-energy formula into a functional of the electron density, Phys. Rev. B 37 (2) (1988) 785.
[31] P.J. Hay, W.R. Wadt, Ab initio effective core potentials for molecular calculations. Potentials for K to Au including the outermost core orbitals, J. Chem. Phys. 82 (1) (1985) 299–310.
[32] K. Liang, et al., Theoretical investigation of the singlet–triplet splittings for carbazole-based thermally activated delayed fluorescence emitters, Phys. Chem. Chem. Phys. 18 (38) (2016) 26623–26629.
[33] T. Yanai, D.P. Tew, N.C. Handy, A new hybrid exchange–correlation functional using the Coulomb-attenuating method (CAM-B3LYP), Chem. Phys. Lett. 393 (1–3) (2004) 51–57.
[34] A.A. Taherpour, M. Jamshidi, O. Rezaei, DFT and TD-DFT theoretical studies on photo-induced electron transfer process on [Cefamandole]. C60 nano-complex, J. Mol. Graph. Model. 75 (2017) 42–48.
[35] P.J. Hay, W.R. Wadt, Ab initio effective core potentials for molecular calculations. Potentials for the transition metal atoms Sc to Hg, J. Chem. Phys. 82 (1) (1985) 270–283.
[36] M. Jamshidi, et al., A highly selective fluorescent chemosensor for Mg2+ ion in aqueous solution using density function theory calculations, J. Mol. Struct. 1123 (2016) 111–115.
[37] S. Dapprich, G. Frenking, Investigation of donor-acceptor interactions: a charge decomposition analysis using fragment molecular orbitals, J. Phys. Chem. 99 (23) (1995) 9352–9362.
[38] X. Su, et al., First-principles study on the bandgap modulation of Be and Mg co-doped ZnO systems, Phys. B Condens. Matter 404 (12–13) (2009) 1794–1798.
[39] R.P. Gangadharan, S.S. Krishnan, Natural bond orbital (NBO) population analysis of 1-Azanapthalene-8-ol, Acta Phys. Pol. 125 (1) (2014).
[40] T. Lu, F. Chen, Atomic dipole moment corrected Hirshfeld population method, J. Theor. Comput. Chem. 11 (1) (2012) 163–183.
[41] S. Tanreh, A. Shameli, E. Balali, Study on sunitinib adsorption on graphene surface as an anticancer drug, J. Appl. Chem. Res. 12 (1) (2018) 79–91.
[42] T. Lu, F. Chen, Multiwfn: a multifunctional wavefunction analyzer, J. Comput. Chem. 33 (5) (2012) 580–592.
[43] B.G. Kim, H.J. Choi, Graphyne: hexagonal network of carbon with versatile Dirac cones, Phys. Rev. B 86 (11) (2012), 115435.
[44] B. Bhattacharya, U. Sarkar, N. Seriani, Electronic properties of homo-and heterobilayer graphyne: the idea of a nanocapacitor, J. Phys. Chem. C 120 (47) (2016) 26579–26587.
[45] M. Perveen, et al., Therapeutic potential of graphitic carbon nitride as a drug delivery system for cisplatin (anticancer drug): a DFT approach, Biophys. Chem. 267 (2020), 106461.
[46] E.C. Dreaden, et al., Size matters: gold nanoparticles in targeted cancer drug delivery, Ther. Deliv. 3 (4) (2012) 457–478.
[47] D.V. Volodkin, A.G. Skirtach, H. Möhwald, Near-IR remote release from assemblies of liposomes and nanoparticles, Angew. Chem. 121 (10) (2009) 1839–1841.
[48] V. Wißdorf, et al., Impedance spectra analysis of p-doped organic thin films by charge carrier distribution evaluation, ACS Appl. Electronic Mater. 1 (10) (2019) 1994–2006.
[49] P.C. Grayson, et al., Positron emission tomography as an imaging biomarker in a prospective, longitudinal cohort of patients with large vessel vasculitis, Arthritis Rheumatol. 70 (3) (2018) 439. Hoboken, NJ.
[50] A. Tariq, et al., DFT study of the therapeutic potential of phosphorene as a new drug-delivery system to treat cancer, RSC Adv. 9 (42) (2019) 24325–24332.
[51] S.-H. Peng, et al., Synthesis of diketopyrrolopyrrole based conjugated polymers containing thieno [3, 2-b] thiophene flanking groups for high performance thin film transistors, Polym. Chem. 8 (22) (2017) 3431–3437.
[52] G. Qu, et al., Improved biocompatibility of black phosphorus nanosheets by chemical modification, Angew. Chem. Int. Ed. 56 (46) (2017) 14488–14493.
[53] A. Eşme, S.G. Sağdınç, Molecular structures, spectroscopic (FT–IR, NMR, UV) studies, NBO analysis and NLO properties for tautomeric forms of 1, 3-dimethyl-5-(phenylazo)-6-aminouracil by density functional method, Spectrochim. Acta Mol. Biomol. Spectrosc. 188 (2018) 443–455.
[54] A. Mohajeri, A. Shahsavar, Tailoring the optoelectronic properties of graphyne and graphdiyne: nitrogen/sulfur dual doping versus oxygen containing functional groups, J. Mater. Sci. 52 (9) (2017) 5366–5379.
[55] M. Lin, et al., Construction of nanoparticle/polymer composite photothermal nanoplatforms and therapeutic applications, Acta Polym. Sin. 2 (2015) 133–146.
[56] R. Hasanzadeh, et al., Sulfonated magnetic nanocomposite based on reactive PGMA-MAn copolymer@ Fe3O4 nanoparticles: effective removal of Cu (II) ions from aqueous solutions, Int. J Poly. Sci. 2016 (2016).